Humidity's influence on visible region refractive index structure parameter C_n^2

Mark P. J. L. Chang, Carlos O. Font, G. Charmaine Gilbreath, and Eun Oh

In the near-infrared and visible bandpasses optical propagation theory conventionally assumes that humidity does not contribute to the effects of atmospheric turbulence on optical beams. While this assumption may be reasonable for dry locations, we demonstrate that there is an unequivocal effect owing to the presence of humidity upon the strength of turbulence parameter, C_n^2, from data collected in the Chesapeake Bay area over 100 m length horizontal propagation paths. We describe and apply a novel technique, Hilbert phase analysis, to the relative humidity, temperature, and C_n^2 data to show the contribution of the relevant climate variable to C_n^2 as a function of time. © 2007 Optical Society of America

OCIS codes: 010.1300, 010.7060, 030.7060.

1. Introduction

It has been known for some time[1] that the scintillation behavior of point sources is a measure of the optical seeing in the atmosphere. What has been less well understood is the contribution of different environmental variables to optical seeing.

Over the past decade, a great deal of study has been dedicated to clarifying this issue. Comprehensive treatments of the theory of wave propagation in random media are given in Tatarskii's seminal works.[2,3] Some of the simplest models based on these complex works are well known and available in the literature: Hufnagel-Valley,[4] SLC-Day and SLC-Night.[5] These models are commonly used to predict the strength of weak clear air turbulence's refractive index structure parameter, C_n^2.

The underlying assumption is that the index of refraction of air depends solely on pressure and temperature at visible and near-infrared wavelengths.[2,6] We can verify this from landbound horizontal path measurements. These show that, during daylight hours on a clear sunny day, the weak scintillation regime C_n^2 trend is dominated by solar insolation, as illustrated in the left-hand plot of Fig. 1.

The right-hand plot of Fig. 1 illustrates the well-known fact that the effects of turbulence do not cease after sunset. Here it is less clear as to the predominant contributing factors. The assumption of temperature dominance is sensible in the driest of environments, but we will demonstrate from experimental evidence that this is an incomplete condition where there is a significant amount of water vapor entering or leaving air volume where C_n^2 is measured.

A. Previous Work

A body of work has been reported whose aims have been to compare bulk climate estimates of C_n^2 with optically derived readings.[7–9] In those works, the wavelengths of the optical measurements were in the mid-infrared (3 to 5 μm), and all showed that humidity along the measurement volume plays a significant role in the temporal behavior of C_n^2.

In a theoretical study of the structure parameter using bulk measurables over sea ice and snow, Andreas[10] defined a refractive index scale n_* via

$$n_* = At_* + Bq_* \rightarrow \frac{n_*}{At_*} = 1 + \frac{Bq_*}{At_*} \qquad (1)$$

where t_* and q_* represent temperature and humidity, scaled such they are constant with height and A and B are constants given in Appendix A. The variable n_* therefore represents a horizontal refractive index layer above the terrestrial surface. He rewrote Eq. (1) in terms of the Bowen ratio Bo, the ratio of sensible

M. P. J. L. Chang (mark@charma.uprm.edu) is with the Department of Physics, University of Puerto Rico, P.O. Box 9016, Mayagüez, Puerto Rico 00681-9016. C. O. Font, G. C. Gilbreath, and E. Oh are with the U.S. Naval Research Laboratory, Washington, D.C. 20375.

Received 9 June 2006; revised 9 November 2006; accepted 11 December 2006; posted 3 January 2007 (Doc. ID 71778); published 9 April 2007.

0003-6935/07/132453-07$15.00/0

Report Documentation Page

Form Approved
OMB No. 0704-0188

1. REPORT DATE	2. REPORT TYPE	3. DATES COVERED
2007		**00-00-2007 to 00-00-2007**

4. TITLE AND SUBTITLE	5a. CONTRACT NUMBER
Humidity's influence on visible region refractive index structure parameter Cn2	5b. GRANT NUMBER
	5c. PROGRAM ELEMENT NUMBER
6. AUTHOR(S)	5d. PROJECT NUMBER
	5e. TASK NUMBER
	5f. WORK UNIT NUMBER
7. PERFORMING ORGANIZATION NAME(S) AND ADDRESS(ES) **Naval Research Laboratory,Code 7215, Remote Sensing Division,4555 Overlook Avenue, SW,Washington,DC,20375**	8. PERFORMING ORGANIZATION REPORT NUMBER
9. SPONSORING/MONITORING AGENCY NAME(S) AND ADDRESS(ES)	10. SPONSOR/MONITOR'S ACRONYM(S)
	11. SPONSOR/MONITOR'S REPORT NUMBER(S)

12. DISTRIBUTION/AVAILABILITY STATEMENT
Approved for public release; distribution unlimited

13. SUPPLEMENTARY NOTES

14. ABSTRACT

15. SUBJECT TERMS

16. SECURITY CLASSIFICATION OF:			17. LIMITATION OF ABSTRACT	18. NUMBER OF PAGES	19a. NAME OF RESPONSIBLE PERSON
a. REPORT	b. ABSTRACT	c. THIS PAGE			
unclassified	**unclassified**	**unclassified**	**Same as Report (SAR)**	**7**	

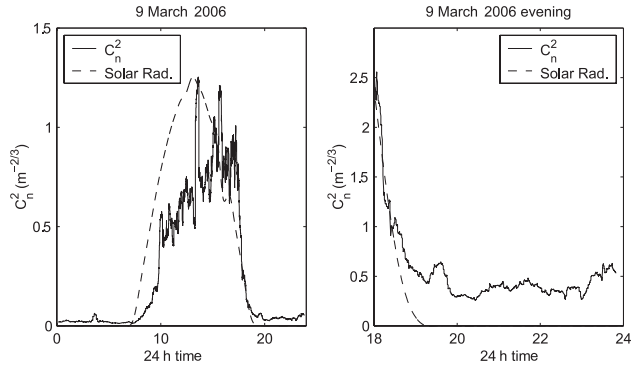

Fig. 1. Effects of solar insolation on C_n^2 as measured on 9 March 2006 in Puerto Rico. Solar radiation measurements are superimposed at an arbitrary scale on top of the C_n^2 data. (Left) The full 24 h period. The vertical axis values are of order $10^{-12}\mathrm{m}^{-2/3}$. (Right) Close up of the evening period. The vertical axis values are of order $10^{-14}\mathrm{m}^{-2/3}$. The C_n^2 data were obtained at an urban site 1.75 km from the sea. These values are in agreement with measurements of seeing over the sea by alternative means (Ref. 23).

heat flux to latent heat flux, such that

$$\frac{n_*}{At_*} = 1 + \left(\frac{\rho c_p}{L}\right)\frac{B}{A(Bo)} = 1 + \left(\frac{B}{KA(Bo)}\right), \qquad (2)$$

where c_p represents the specific heat of air at constant pressure, L is the latent heat of the sublimation of ice, and ρ is the air density. Since $Bo \propto t_*/q_*$, this formulation allows the dependence of the refractive index scale on temperature and humidity scales to be easily interpreted.

We adapt Eq. (2) to our experimental conditions by setting L to be the latent heat of vaporization of water, and we assume that $P = 1000$ hPa, $T = 25$ °C, and $\lambda = 0.93$ μm. The result is shown in Fig. 2; from this it is clear that, when $|Bo|$ is large, n_*/At_* is near 1. This means that, when sensible heat (heat exchange without change of thermodynamic phase) dominates the Bowen ratio, the t_* in the denominator of Eq. (1) is the principal parameter.

When $|Bo|$ is small, however, the latent heat flux dominates, and q_* makes the major contribution to n_*. Thus there is an interplay between humidity and

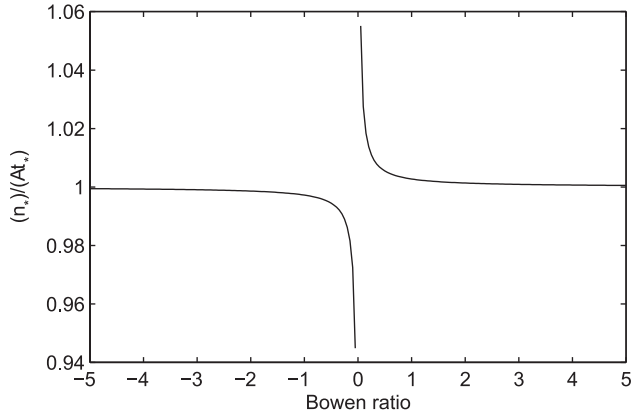

Fig. 2. Graph of $n_*/(At_*)$ versus Bowen ratio for $\lambda = 0.93$ μm.

temperature effects on the refractive index in the visible and near infrared, which varies as a function of the Bowen ratio. The pole at the origin of Fig. 2 is indicative of a breakdown of this formulation at very small Bowen ratios. Nevertheless the curve strongly suggests that, as long as there is significant injection of moisture into the measurement volume of C_n^2, the humidity effects become nonnegligible.

Here we demonstrate that the temporal behavior of the optically determined turbulence structure parameter C_n^2 in the visible and near-infrared bandpasses at a coastal site is strongly influenced by local humidity. Although no Bowen ratio values could be determined from the available measurements, the results do support the qualitative interpretation of Andreas's work.

2. Experiment and Correlogram Analysis

The C_n^2 and associated weather variable data used in this study were collected over a number of days during 2003 and 2004 at Chesapeake Beach in Maryland, USA. The C_n^2 data were obtained with a commercially available scintillometer [Model LOA-004, Optical Scientific, Gaithersburg, Maryland], which served as both a scintillometer and as an optical anemometer for winds transverse to the beam paths. The separation between source and receiver was just under 100 m, placing the system in the weak scintillation regime. The local weather parameters were determined by a Davis Provantage Plus (DP+) weather station. The LOA-004 had a sample rate of 10 s, and the DP+ was set at 5 min.

The LOA-004 comprises a single modulated infrared transmitter whose output is detected by two single pixel detectors. The transmitting LED has a bandwidth of 0.92 to 0.96 μm, while the detector bandwidth is much broader, at 0.65 to 1.0 μm. The path-integrated C_n^2 measurements are determined by the LOA-004 by computation from the log-amplitude scintillation $[C_\chi(r)]$ of the two receiving signals.[11,12] The algorithm for relating $C_\chi(r)$ to C_n^2 is based on an equation for the log-amplitude covariance function in Kolmogorov turbulence by Clifford *et al.*[13]

The C_n^2 data were smoothed with a 60 point (5 min) rolling average function. We define the morning and night portions of a 24 h period with respect to the measured solar irradiance function such that we exclude the effect of solar insolation from the data in this study. Morning runs from midnight until sunrise, while night runs from sunset until 23:59. As reported in Oh *et al.*[14–16] visual inspection of the time series data gives the impression that there is an approximate inverse relationship between C_n^2 and relative humidity. This can be appreciated in a more quantitative manner by graphing one parameter against the other.

We chose data sets in which the temperature variations are no more than 16 °F, and the pressure change is at most 15 hPa over the time intervals of interest. The actual range of variation per data set is shown in Table 1. The data sections were also se-

Table 1. Mean and Range of Bulk Parameter Measurements and the Maximum Range of Specific Humidity (Δ_{Q_s})

Date	$\overline{RH}$ (%)	$\overline{T}$ (°F)	$\overline{P}$ (hPa)	Δ_{RH}	Δ_T	Δ_P	Δ_{Q_s} (g/kg)
11/03/03 (p.m.)	83.6	65.2	1015.3	15	2	0.4	2.2
11/09/03 (a.m.)	49.3	38.8	1030.9	11	3.1	1.2	0.5
11/10/03 (a.m.)	76.4	46.8	1027.6	11	8	1.8	0.6
02/02/04 (a.m.)	91.4	29.9	1022.9	16	2.5	6.6	0.8
03/27/04 (p.m.)	76.4	46.8	1027.6	11	8	1.8	1.7
03/28/04 (a.m.)	71	44.5	1027.6	16	0.7	0.6	0.9
04/03/04 (a.m.)	76.1	46.6	997.4	18	5.9	4.9	0.4
04/03/04 (p.m.)	43	40.1	1004.5	14	5.6	2.1	1.1

lected to have no scattering effects attributable to snow or rain, and the wind was northerly (to within approximately ±20°, inflowing from the bay to land). Only a small subset of eight morning and evening runs, spanning seven days between November 2003 and March 2004, provided a complete time series in both ambient weather variables and C_n^2. Part of this is shown in Fig. 3; the C_n^2 versus humidity correlograms evidence a negative gradient in all eight runs. Table 1 shows us that the relative humidity variation is more strongly reflective of changes in absolute moisture content than of moisture holding capacity of the air.

We conclude that humidity plays a significant part in the behavior of the refractive index structure parameter C_n^2 in the data sets studied.

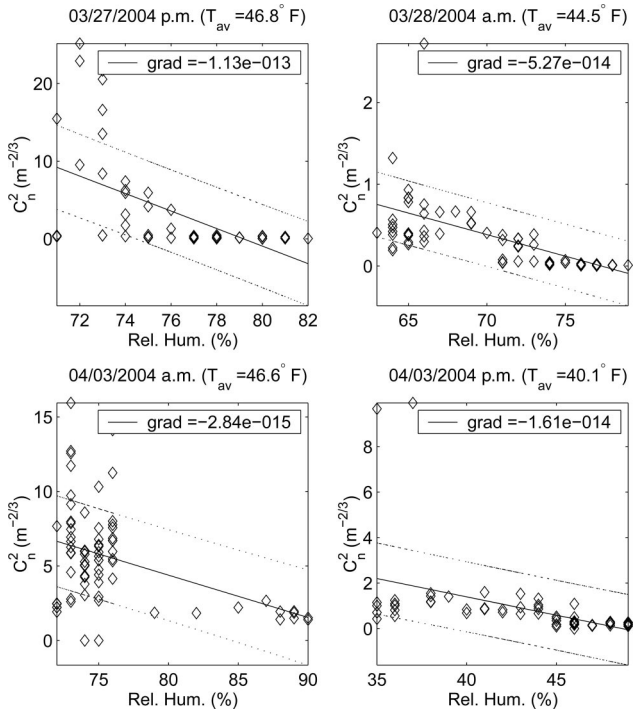

Fig. 3. Example correlograms of C_n^2 and relative humidity in the absence of solar insolation. The upper and lower bounds indicate the 50% confidence level. The C_n^2 magnitudes are $10^{-15}\mathrm{m}^{-2/3}$, in agreement with measurements of seeing over the sea by alternative means (Ref. 23).

3. Stationarity Problem

The unsophisticated use of the correlogram tool in Section 2 is a rapid, first-order method for inferring the statistical influence of one measurable upon another. However it is unsatisfactory as it does not reveal any detailed information such as exactly when the humidity contribution is important with respect to all other possible parameters (e.g., temperature) and to what degree its contribution is influential. Cross-covariance techniques are a possible second-order method[17] for extending the analysis, but there are two major stumbling blocks. The first is the difficulty in interpreting the meaning of the covariance functions physically, and the second is the nonstationary nature of the data. In the latter case it is well known that strict stationarity is a constraint that is impossible to satisfy on practical grounds since no detector can cover all possible points in phase space. This has motivated us to employ a novel analysis technique to infer the relationship between C_n^2 and the climate parameters, which we briefly describe in the following section. We leave a more detailed study of the limitations of the technique to a separate paper.

A. Analytic Signal

Gabor[18] defined the complex analytic signal, namely,

$$\Psi(t) = X(t) + iY(t),$$

where

$$Y(t) = \mathcal{H}[X(t)] = \frac{-1}{\pi}\,\mathbf{P}\int_{-\infty}^{\infty}\frac{X(\tau)}{(t-\tau)}\,\mathrm{d}\tau, \qquad (3)$$

where $\mathcal{H}[\bullet]$ represents a Hilbert transform. Through this definition, $\Psi(t)$ is unique. The Hilbert transform is a well-known integral transform with a singular kernel $(1/[\pi(t-\tau)])$, τ also being a time variable if t is time. It is also a Cauchy principal integral, which we denote by $\mathbf{P}$. Note that the Hilbert transform preserves the norm of the real signal; the difference between Y and X is a $\pi/2$ phase shift for a periodic function. That is, the Hilbert transform of $\cos t$ is $\sin t$, and $\sin t$ is $-\cos t$, and the transform of a constant is zero.

Equation (3) means that we can write the analytic signal as

$$\Psi(t) = a(t)\exp^{i\Phi(t)}, \quad \text{where } a(t) = \sqrt{X^2(t) + Y^2(t)},$$
$$\Phi(t) = \arctan\left(\frac{Y(t)}{X(t)}\right), \qquad (4)$$

which is similar to the well-known Fourier expression. We may now determine the instantaneous signal phase, $\Phi(t)$. Thus we can also calculate the instantaneous frequency $\omega(t)$, defined as

$$\omega(t) = \frac{d\Phi(t)}{dt}. \quad (5)$$

Both $\Phi(t)$ and $\omega(t)$ can be interpreted as physical measurables provided certain preconditions, which we describe below, are met.

B. Hilbert Phase Analysis

There is a problem with the definition of Eq. (3); the Hilbert transform's kernel represents a noncausal filter, of infinite support. So if one applies the Hilbert transform directly to a time-varying signal that has a nonzero local mean in any subsection, there is a high probability that at least one of a number of paradoxes[19] will be encountered. This may be best appreciated if we consider a signal in phase space, as in the left-hand plot of Fig. 4. Here we show the real versus the imaginary components of the Hilbert transform of a series of analytic C_n^2 measurements. The trajectory of the analytic signal's vector is subject to many alterations in the vector start point, norm, and phase angle. Any attempt to determine the instantaneous frequency is bound to be problematic as we are not able to follow the signal vector's start position over time; this starting point obviously does not remain at the origin of the coordinate system. Calculating the instantaneous frequency from the Hilbert transform as is will generate both positive and negative values, rendering it physically uninterpretable.

The paradoxes may be avoided by application of the empirical mode decomposition (EMD) method developed by Huang *et al.*,[20] which we have implemented.[21,22] EMD is a unique and novel method that is able to separate an arbitrary real-time series into eigenfunctions termed intrinsic mode functions or IMFs, each of which possesses a structure with well defined instantaneous frequencies, $\omega(t)$. The term eigenfunction is used suggestively here; we do not mean to imply that the IMFs are eigenfunctions in the strict sense.

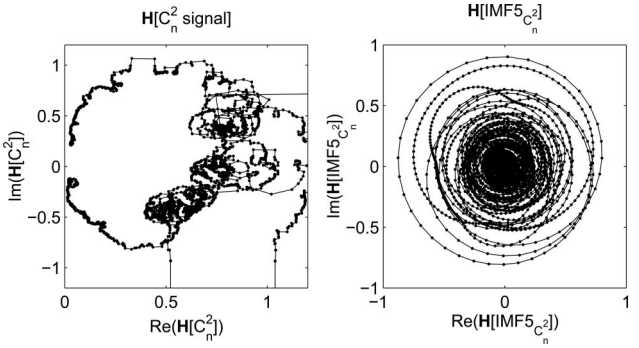

Fig. 4. (Left) Hilbert phase space plot of the trajectory of the C_n^2 signal vector of Fig. 1. The signal vector's start point drifts arbitrarily around the phase space making the determination of a physically reasonable instantaneous frequency impossible over the whole path. (Right) Hilbert phase space plot of the trajectory of a single IMF derived from the C_n^2 signal. The IMF vector's start point is stable, and its trajectory does not change direction, so a positive instantaneous frequency can be determined at all points.

Briefly, the EMD technique consists of (1) the determination of two envelope functions about the time series covering all the local minima and maxima, respectively; (2) the computation of the mean of the two envelope functions; (3) the removal of the mean of the envelopes from the time series in an iterative manner until the mean is found to be zero; and (4) storing of the resulting mode as an IMF. The IMF is then subtracted from the original time series and steps (1) to (4) are repeated, thereby sifting out a family of IMFs, stopping only when the resulting mode shows no variation. The final mode represents the overall trend of the signal and is not itself an IMF.

The Hilbert transform of the IMFs, one of which is shown on the right-hand side of Fig. 4, ensures that the analytic signal vector's origin stays fixed and no sudden changes in the direction of $\omega(t)$ occur. These conditions being satisfied, the instantaneous frequency remains positive and physically meaningful.

4. Hilbert Phase Analysis

The Hilbert phase analysis (HPA) technique is based on the ideas mentioned in the previous subsections. It is clear that a phase angle $[\Phi(t)]$, as well as an amplitude $[a(t)]$, can be found from the Hilbert transform of the IMFs derived from the EMD sifting process.

The procedure for the HPA data analysis follows a three-step protocol:

1. Decompose the time series measurements of differing parameters via EMD, obtaining their IMFs and trend lines.
2. Apply the Hilbert transform to the various IMF sets. We discard the trend lines as the reason that the original time series fail to be Hilbert transformed in a physically comprehensible manner.
3. Examine the instantaneous phase angles of the Hilbert transformed IMFs between different parameters to infer the dynamics of the physical system.

A. Interpretation of Hilbert Phase Analysis

Here we demonstrate that the physical effects of a nonlinear, nonstationary, time-varying system can be studied via the sum of all IMF phases, $\sum_{\mathrm{IMF}} \Phi(t)$.

In Fig. 5 the $\sum_{\mathrm{IMF}} \Phi(t)$ is graphed with the solar radiation data superimposed for example days. There is clearly a gradient change in the phase function at sunrise and sunset. Also notable is the phase jump toward a lower gradient whenever the solar radiation function exhibits a drop in amplitude; likewise the phase gradient increases with sudden increases in the measured solar radiation. This can be understood as a reduction in energy in the system leading to a lower instantaneous frequency, therefore we see a lower phase gradient. A change in energy results in a change in instantaneous frequency, so we see a modified gradient.

We conclude that the overall physical features of a nonstationary time series can be extracted by an inspection of the sum of its Hilbert phases of the IMFs.

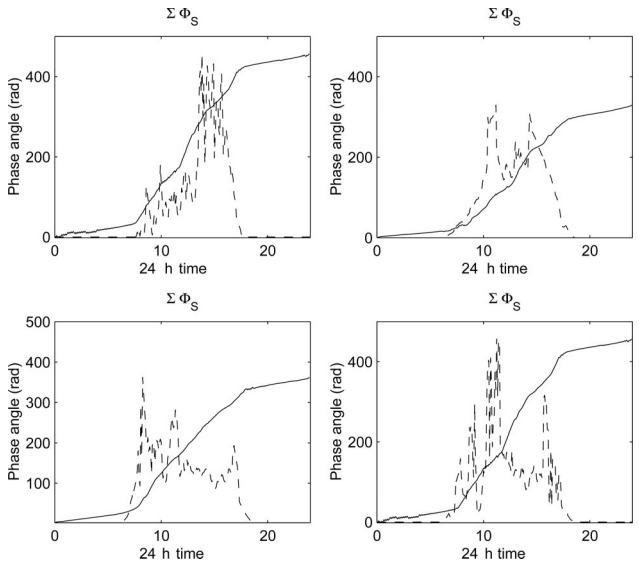

Fig. 5. Sum of all Hilbert phases of the measured solar radiation IMFs ($\sum\Phi_S$) for the following days: 2 February, 27 March, 28 March, and 3 April 2004. The solar radiation is superimposed at an arbitrary scale.

5. Hilbert Phase Analysis of C_n^2, Humidity and Temperature

A. Phase Locking Between Measurables

To better understand the dependence of Φ_C upon humidity and temperature, we consider the difference between observable phases, as illustrated in Fig. 6. We define the following difference terms:

$$\Delta_{CT} = \sum \Phi_C - \sum \Phi_T, \qquad \Delta_{CH} = \sum \Phi_C - \sum \Phi_H,$$

$$\Delta_{C\overline{HT}} = \sum \Phi_C - \frac{\left(\sum \Phi_H + \sum \Phi_T\right)}{2}, \tag{6}$$

representing the phase differences between C_n^2 and the bulk climate parameter. It is anticipated that the controlling climate parameter will be indicated by a near-zero difference Δ. We reason this because if Δ is constant between C_n^2 and a climate variable then the two data sets must be phase locked. If the mean Δ is zero, then any variations about zero should indicate a synchronization between data sets.

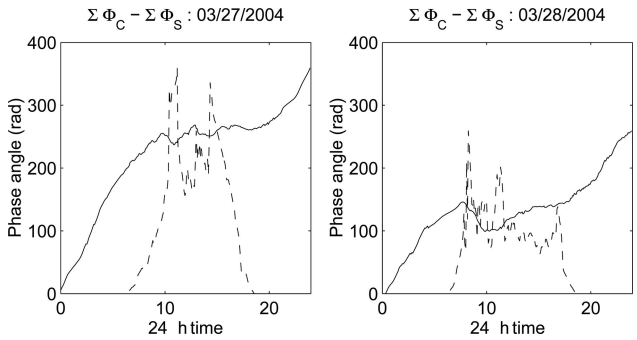

Fig. 7. Plots of Hilbert phase differences between C_n^2 and solar radiation for 27 and 28 March 2004. The solar radiation function is superimposed at an arbitrary scale on each graph. Note the flattening out of the phase difference function during the daylight hours.

Supporting empirical evidence is found upon studying cases wherein the solar insolation influence upon the measured C_n^2 is strong, as in Fig. 7. In those plots one can see that the difference between the summed Hilbert phase of C_n^2 and solar radiation ($\sum\Phi_C - \sum\Phi_S$) flattens out when the solar function is significant.

Motivated by this, we determined by linear regression the mean gradients of all the Δ curves, which we list in Table 2. If we assume that the only major contributor should be the local temperature variations, Δ_{CT} should be zero or near-zero in all cases. This turns out not to have occurred. In fact, Δ_{CT} has no near-zero value, so temperature variation cannot be said to be phase locked with the refractive index structure parameter.

If humidity has a controlling effect in the visible and near-infrared, then it should exhibit a range of values near zero for Δ_{CH}. It does so only for 10 November 2003 (a.m.) and 28 March 2004 (a.m.). It is noteworthy that 9 November 2003 shows a possible phase lock between the mean of humidity and temperature with C_n^2. This seems to indicate that that temperature is vying with humidity for influence over the C_n^2 parameter during that morning.

B. Further Study

If we define "dominance" to mean that the phase gradient is the value closest to zero of the differences under scrutiny then we find that humidity is domi-

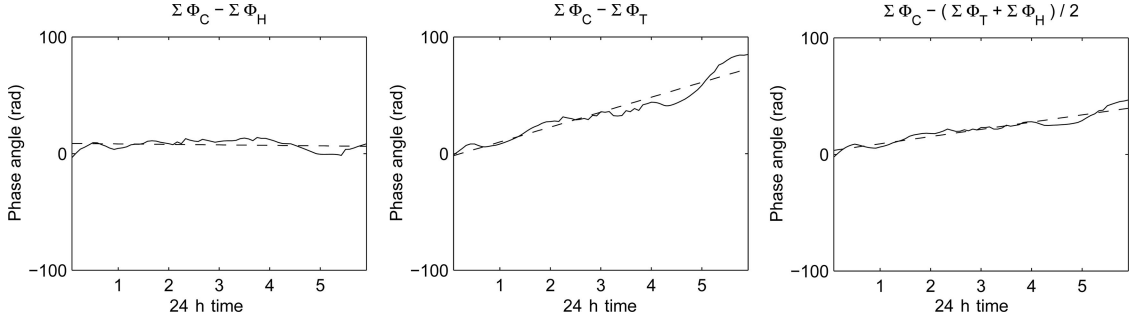

Fig. 6. Difference plots for the morning of 10 November 2003. The dotted line is a linear regression, estimating the mean phase gradient. The leftmost graph shows a phase lock between C_n^2 and relative humidity.

Table 2. Linear Regression Line Gradients of the Phase Differences

Date	Δ_{CH}	Δ_{CT}	$\Delta_{C\overline{HT}}$
11/03/03 (p.m.)	−9.7(4)	−8.0(0)	−8.8(7)
11/09/03 (a.m.)	−11.2(4)	9.7(7)	−0.7(4)
11/10/03 (a.m.)	−0.4(1)	12.7(9)	6.1(9)
02/02/04 (a.m.)	8.5(1)	−12.3(0)	−1.8(9)
03/27/04 (p.m.)	3.7(6)	28.1(7)	15.9(7)
03/28/04 (a.m.)	0.0(2)	−3.3(1)	−1.6(5)
04/03/04 (a.m.)	6.8(1)	6.6(8)	6.7(4)
04/03/04 (p.m.)	−27.3(3)	−2.3(3)	−14.8(3)

nant for the 10 November 2003, 2 February 2004, 27 March 2004, and 28 March 2004 data sets. The 3 November 2003 and 3 April 2004 (a.m. and p.m.) data sets show that $\Delta_{CT} < \Delta_{CH}$, indicating the dominant effect is temperature, this being extremely strong for the 3 April 2003 (p.m.) data set and rather weaker for the other two. We postulate that the 3 November 2003 and 3 April 2004 data sets indicate that both temperature and humidity contribute to the behavior of C_n^2, with the HPA method possibly showing the proportional contribution to C_n^2 of each climate variable. This is clearly an area to be examined further.

6. Conclusion

From experimental data we have shown conclusively that humidity plays a significant part in the visible and near-infrared measure of C_n^2 in a coastal environment. This is in qualitative agreement with Andreas's model and is a natural extension of the results from the mid-infrared.

Furthermore we have explored a new technique, the Hilbert phase analysis, with which to study this physical phenomenon. In overall terms, the HPA method is in agreement with the correlogram results. Phase locking between data is an unexpected result that needs further examination. We have found that the HPA technique described here is very promising and is likely to provide much more information about the changes to a physical system than traditional methods.

Appendix A. Definitions

The constants A and B of Eq. (1) in the 0.36 to 3 μm wavelength region are

$$A = -10^{-6} m_1(\lambda)(P/T^2),$$

$$B = 4.6150 \times -10^{-6}[m_2(\lambda) - m_1(\lambda)]. \quad \text{(A1)}$$

P and T are the ensemble average air pressure and temperature, respectively. The functions m_1 and m_2 are polynomials in wavenumber given by

$$m_1(\lambda) = 23.7134 + \frac{6839.397}{130 - (1/\lambda)^2} + \frac{45.473}{38.9 - (1/\lambda)^2},$$

$$m_2(\lambda) = 64.8731 + 0.58058(1/\lambda)^2 - 0.0071150(1/\lambda)^4 + 0.0008851(1/\lambda)^6, \quad \text{(A2)}$$

with λ units in micrometers.

M. P. J. L. Chang thanks Norden Huang, Haedeh Nazari, and Erick Roura for illuminating discussions. This work was supported in part by the Office of Naval Research.

References

1. F. Roddier, "The effects of atmospheric turbulence in optical astronomy," Prog. Opt. **XIX,** 281–377 (1981).
2. V. Tatarskii, *Wave Propagation in a Turbulent Medium* (McGraw-Hill, 1961).
3. V. Tatarskii, *The Effects of a Turbulent Atmosphere on Wave Propagation* (Israel Program for Scientific Translations, 1971).
4. R. R. Beland, *Propagation through Atmospheric Optical Turbulence* (SPIE Optical Engineering Press, 1993).
5. M. Miller and P. L. Zieske, *Turbulence Environmental Characterization,* RADC-TR-79-131, ADA072379 (Rome Air Development Center, 1976).
6. M. C. Roggeman and B. Welsh, *Imaging through Turbulence* (CRC Press, 1996).
7. P. A. Frederickson, K. L. Davidson, C. R. Zeisse, and C. S. Bendall, "Estimating the refractive index structure parameter (C_n^2) over the ocean using bulk methods," J. Appl. Meteorol. **39,** 1770–1783 (1999).
8. K. L. Davidson, G. E. Schacher, C. W. Fairall, and A. K. Goroch, "Verification of the bulk method for calculating overwater optical turbulence," Appl. Opt. **20,** 2919–2924 (1981).
9. G. J. Kunz, M. M. Moerman, P. J. Fritz, and G. de Leeuw, "Validation of a bulk turbulence model with thermal images of a point source," in *Image Propagation through the Atmosphere,* C. Dainty and L. R. Bissonnette, eds., Proc. SPIE **2828,** 108–116 (1996).
10. E. L. Andreas, "Estimating C_n^2 over snow and sea ice from meteorological data," J. Opt. Soc. Am. A **5,** 481–494 (1988).
11. G. R. Ochs and T.-I. Wang, "Finite aperture optical scintillometer for profiling wind and C_n^2," Appl. Opt. **17,** 3774–3778 (1979).
12. T.-I. Wang, "Optical flow sensor," U.S. patent 6,369,881 (9 April 2002).
13. S. F. Clifford, G. R. Ochs, and R. S. Lawrence, "Saturation of optical scintillation by strong turbulence," J. Opt. Soc. Am. **64,** 148–154 (1974).
14. E. Oh, J. Ricklin, F. Eaton, C. Gilbreath, S. Doss-Hammell, C. Moore, J. Murphy, Y. H. Oh, and M. Stell, "Estimating optical turbulence using the PAMELA model," in *Remote Sensing and Modeling of Ecosystems for Sustainability,* W. Gao and D. R. Shaw, eds., Proc. SPIE **5550,** 256–266 (2004).
15. S. Doss-Hammel, E. Oh, J. C. Ricklin, F. D. Eaton, G. C. Gilbreath, and D. Tsintikidis, "A comparison of optical turbulence models," in *Remote Sensing and Modeling of Ecosystems for Sustainability,* J. C. Ricklin and D. G. Voelz, eds., Proc. SPIE **5550,** 236–246 (2004).
16. E. Oh, J. C. Ricklin, G. C. Gilbreath, N. J. Vallestero, and F. D. Eaton, "Optical turbulence model for laser propagation and imaging applications," in *Free-Space Laser Communication and Active Laser Illumination III,* D. G. Voelz and J. C. Ricklin, eds., Proc. SPIE **5160,** 25–32 (2004).
17. C. O. Font, M. P. J. L. Chang, E. Oh, and C. Gilbreath, "Humidity contribution to the refractive index structure function C_n^2," in *Atmospheric Propagation III,* C. Y. Young and G. C. Gilbreath, eds., Proc. SPIE **6215,** 621502 (2006).
18. M. Born and E. Wolf, *Principles of Optics,* 7th ed. (Cambridge U. Press, 1999).
19. L. Cohen, *Time Frequency Analysis* (Prentice Hall, 1995).
20. N. E. Huang, Z. Shen, S. R. Long, M. C. Wu, H. H. Shih, Q. Zheng, N.-C. Yen, C. C. Tung, and H. H. Liu, "The empirical mode decomposition and the Hilbert spectrum for nonlinear and nonstationary time series analysis," Proc. R. Soc. London Ser. A **454,** 903–995 (1998).

21. M. P. J. L. Chang, E. A. Roura, C. O. Font, C. Gilbreath, and E. Oh, "Applying the Hilbert–Huang decomposition to horizontal light propagation C_n^2 data," in *Advances in Stellar Interferometry,* J. D. Monnier, M. Schoeller, and W. C. Danchi, eds., Proc. SPIE **6268,** 62683E (2006).
22. C. O. Font, M. P. J. L. Chang, E. Oh, and C. Gilbreath, "On the relationship between C_n^2 and humidity," in *Advances in Stellar Interferometry,* J. D. Monnier, M. Schoeller, and W. C. Danchi, eds., Proc. SPIE **6268,** 62683D (2006).
23. H. Beaumont, C. Aime, E. Aristidi, and H. Lantéri, "Image quality and seeing measurements for long horizontal overwater propagation," Pure Appl. Opt. **6,** 15–30 (1997).